Disequilibrating Dynamic Polymers for Spontaneous Recyclability

Yuanxin Deng[1], Ling Liu[1], Hong-Xi Luo[2], He Tian[1], Da-Hui Qu[1]*, Ben L. Feringa[1,3]*, Qi Zhang[1]*

[1]*Key Laboratory for Advanced Materials and Joint International Research Laboratory of Precision Chemistry and Molecular Engineering, Feringa Nobel Prize Scientist Joint Research Center, Institute of Fine Chemicals, Frontiers Science Center for Materiobiology and Dynamic Chemistry, School of Chemistry and Molecular Engineering, East China University of Science and Technology; Shanghai 200237, China.*

[2] *Andlinger Center for Energy and the Environment, Princeton University, Princeton, NJ 08540, USA.*

[3] *Stratingh Institute for Chemistry and Zernike Institute for Advanced Materials, Faculty of Science and Engineering, University of Groningen; Nijenborgh 4, 9747 AG Groningen, The Netherlands.*

*Correspondence to: dahui_qu@ecust.edu.cn; b.l.feringa@rug.nl; q.zhang@ecust.edu.cn

Abstract:

Chemical recycling of synthetic polymers is key to our future circular plastics economy[1–3]. Current chemical solutions rely on either catalyst design or introducing weak bonds.[4–6] The former approach doesn't tackle the thermodynamic trap of conventional plastics, while the latter usually compromises materials performances. Despite recent advances in ring-strain engineering of lactone-based polymers allowing catalyst-enabled recyclability,[1,6,7] polymer-to-monomer recycling processes under mild, waste-free, and cost-affordable conditions remain a formidable challenge. Here, we report an intrinsically recyclable polymer disequilibrated by kinetic control of bulk reconstruction mediated with dynamic bonds, enabling spontaneous polymer-to-monomer conversion by direct solid-to-solid (crystal) transition. The key feature of the system is to couple two types of dynamic chemical equilibria, i.e., noncovalent self-assembly of side-chains and dynamic covalent polymerization of mainchains. We discovered that controlling the sidechain H-bond stacking geometry could be used to spatially separate the polymerizing moieties of monomers in the solid state and bias the monomer/polymer equilibrium toward the direction of depolymerization. As a result, a semi-crystalline, Nylon-like, and easy-to-prepare polymeric material can be spontaneously recycled into crystalline monomers using a mild thermal activation process (120°C), featuring quantitative recycling yield, high monomer purity (over 90%) at low-cost while avoiding the use of any solvent or catalyst during recycling. Life-cycle assessment shows a remarkably advantageous environmental footprint of this technology compared with solvent-based chemical recycling routes. These findings offer a supramolecular solution towards cost-effective closed-loop recycling of covalent polymers.

Traditional plastics have been optimized for decades to maximize the polymerization ability[8], i.e., Gibbs free energy change ($\Delta G_p°$), to gain quantitative monomer conversion, which, in contrast, makes the depolymerization process of the "thermodynamically trapped" material inherently difficult and energy-consuming. For example, poly(ethylene) requires high temperature (ceiling temperature over 600°C) to offer sufficient entropy driving force to compete with the very high enthalpy change ($\Delta H_p°$) involved in polymerization,[9] thus enabling spontaneous polymer-to-monomer depolymerization (Fig. 1a). Hence, by molecularly engineering the monomer structures to balance the polymerization/depolymerization abilities,[1] chemists have designed a family of synthetic polymers that can be recycled under relatively mild conditions.[10–20] The key design feature is to lower the polymerization reactivity ($\Delta G_p°$), thus increasing the depolymerization propensity of the resulting polymers to enable spontaneous polymer-to-monomer conversion without the need for extreme temperatures. Pioneering efforts especially on lactone-based poly(ester)s have been using the "near-equilibrium" design strategy (Fig. 1b),[21] enabling the subtle balance between polymerization and depolymerization abilities by delicate control of the ring strain of the lactone monomers. Despite the versatility of this molecular engineering strategy, it usually trades off the polymerization efficiency due to the nature of near-equilibrium reactions to achieve efficient monomer conversion, and costs of energy and solvents to take advantage of entropy as the driving force.[22] On the other hand, supramolecular polymers offer intrinsically dynamic polymeric systems with full-cycle circularity, yet are limited in mechanical robustness akin to conventional plastics. Therefore, it remains a fundamental challenge to design dynamic polymers with closed-loop chemical recyclability featuring minimum energy consumption while being highly environmental benign in a full life cycle without compromising material properties like robustness.[23,24]

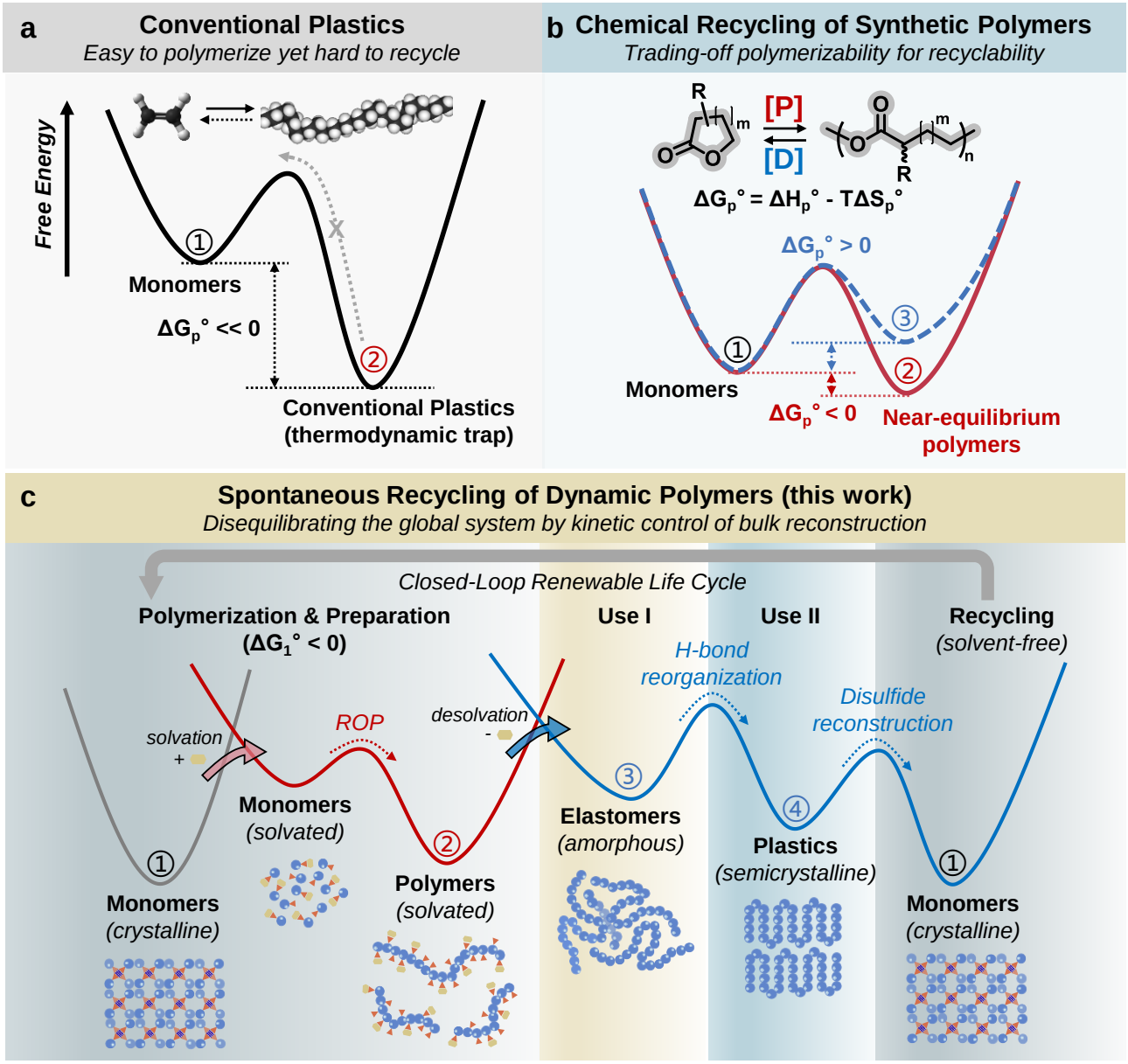

Fig. 1 | Conceptual illustration of the energy landscape of conventional plastics and chemically recyclable polymers. a, Conventional polymers are too stable to be readily recycled due to the very negative $\Delta G_p°$; **b**, Near-equilibrium polymers are a family of ring-opening polymers with moderate ring strain that polymerize at low temperature ② and recycle at elevated temperature ③; **c**, The disequilibrating strategy in this work starts with inherently stable monomer crystals, produce metastable polymers by kinetic control of a solvation/desolvation process, and process the materials by spontaneous evolution from amorphous elastomers to semicrystalline plastics and eventually self-recycle back to original monomers to close the loop. Compared with near-equilibrium design, the disequilibrating strategy allows thermodynamically spontaneous polymer-to-monomer recycling without external energy compensation.

Here we propose a supramolecular strategy to disequilibrate the dynamic polymeric system in which monomers are thermodynamically stabilized by supramolecular self-assembly in the solid states, while solvent-free polymers are kinetically prepared and stabilized by a solvation-desolvation cycle, to serve as a robust material with a certain life cycle span for specific applications, and eventually go to the equilibrated monomer state at the melting temperature in a spontaneous and catalyst-free way. To test our unique approach we used thioctic acid (TA) derivatives which are known for their polymerization ability and structural feature combining dynamic covalent bonds and noncovalent bonds to form poly(TA) network by neat ring-opening polymerization (ROP). [25] However, we discovered that the corresponding primary amide derivative, i.e., thioctic amide (TAA), didn't show common ROP in its neat state to form polymers. Instead, the TAA melts quickly recrystallized into plate-like monomeric crystals (Fig. 2a). This uncommon phenomenon intrigued us and thus we carefully analyzed the solid-state structure of TAA (Fig. 2b and Supplementary Fig. 1). As a result, the unique H-bond self-assembled geometry of TAA in crystals is the decisive factor: The primary amide bonds dominate the supramolecular self-assembly of TAA and result in a special cross-stacking architecture of the 1,2-dithiolane rings, which spatially isolates the monomer units, i.e., the 1,2-dithiolane rings, and thus prevents the intermolecular disulfide exchange, key to intermolecular ROP, while facilitating the intramolecular ring-closing reaction. We envisioned that once one could readily modulate the sidechain H-bonds and disequilibrate the dynamic covalent ROP reaction of the mainchain, it is possible to obtain the kinetically stablized polymers, which are inherently capable of self-recycling into the thermodynamic products, i.e., the original monomers, to close the recycling loop.

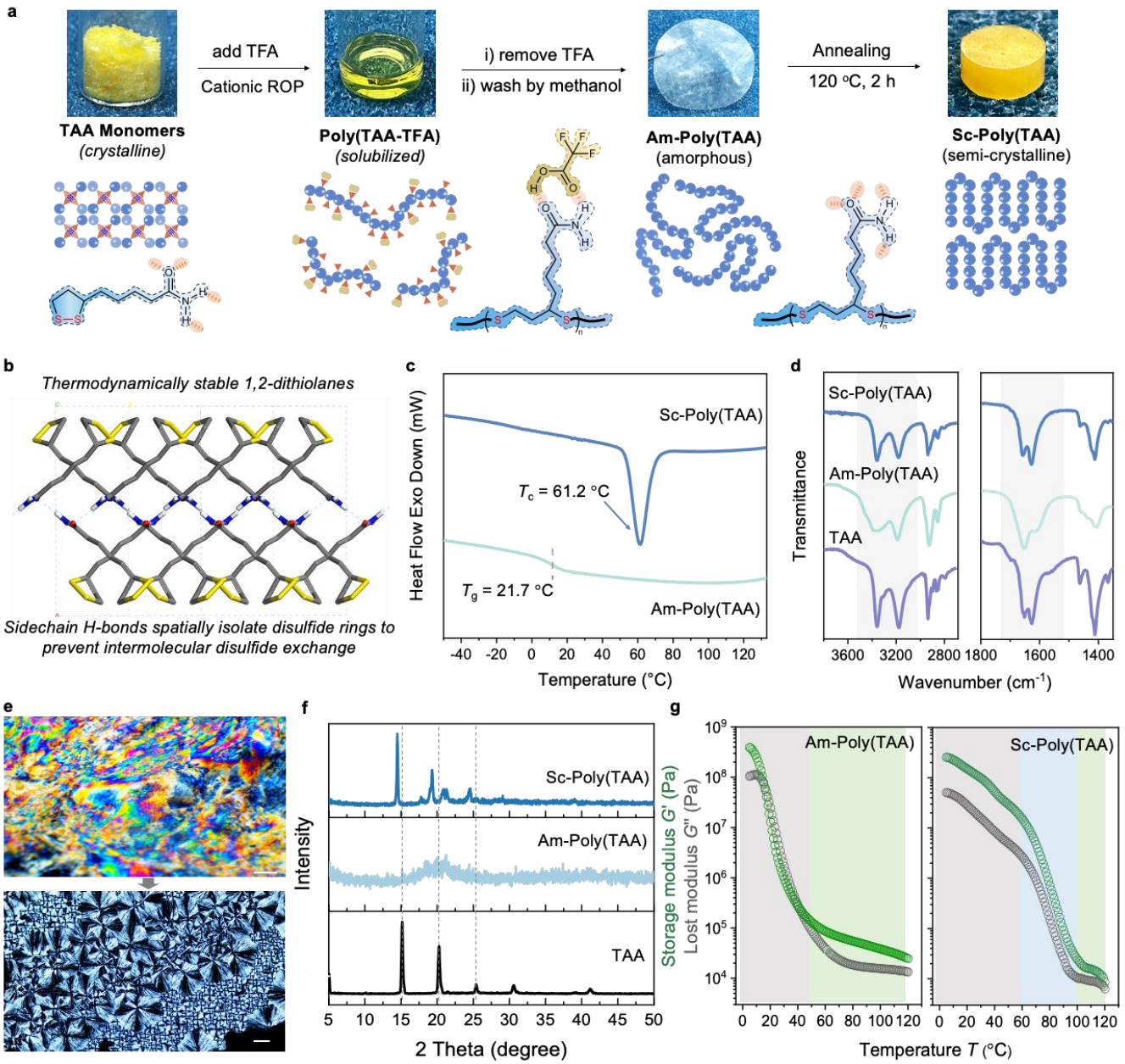

Fig. 2 | Structure characterization of poly(TAA). **a**, Preparation method of Am-poly(TAA) and Sc-poly(TAA) and photographs of the resulting polymer. **b**, X-ray single-crystal structure of TAA monomer. **c**, DSC measurement of poly(TAA). **d**, Partial ATR spectra of TAA monomer, Am-poly(TAA), and Sc-poly(TAA). **e**, POM images of Am-poly(TAA) (up, scare bar refers to 100 μm) and Sc-poly(TAA) (down, scare bar refers to 50 μm). **f**, XRD patterns of TAA monomer and polymers. **g**, Temperature-dependent storage moduli of polymers recorded by rheometer under a constant frequency of 1 Hz.

To search for the H-bond modulator (Fig 2a), a group of small-molecule additives featuring H-bond competitors have been examined (Supplementary Fig. 2,3), and trifluoroacetic acid (TFA) was eventually selected as the ideal one because: i) It is an excellent solvent for TAA due to its strong H-bonding ability; ii) Due to the volatile it is easily removable under vacuum; iii) Catalyzing disulfide exchange reactions to enable efficient ROP of TAA at high concentrations. Therefore, we managed to prepare poly(TAA) polymers by using TFA as the supramolecular modulator. The strong solvation effect of TFA inhibited the H-bond stacking of TAA monomers, and thus recovered the polymerizability to yield poly(TAA). The high volatility of TFA allows an energy-saving desolvation to yield solvent-free poly(TAA), which could be isolated and purified as a dry colorless film after removal of most of TFA under vacuum and subsequent methanol washing to remove the residual TFA and monomer (Fig. 2a). The as-prepared poly(TAA) materials showed a glassy transition temperature (T_g) at 21.7°C (Fig. 2c) and swellability in polar solvent (Supplementary Figs. 3, 4). Further analysis of ^{1}H NMR and matrix-assisted laser desorption ionization time-of-flight mass spectrometry (MALDI-TOF-MS) (Supplementary Figs. 5–7) confirmed the chemical nature of poly(disulfide)s. Attenuated total reflectance infrared (ATR-IR) spectroscopy was further used to characterize the distinctive amide bonds in the polymers, showing the co-existence of disordered and ordered H-bond crosslinks in the network (Fig. 2d). The resulting poly(TAA) polymers could be processed into a translucent film at room temperature, exhibiting an elastomer-like stress-strain curve in tensile experiment with Young's modulus of 235 MPa (Supplementary Fig. 8), which was as strong as the state-of-the-art poly(disulfide)s crosslinked by the reticular H-bonds of acylhydrazine units[26].

The resulting poly(TAA) film bears nano-crystalline domains in the bulk phase as observed by polarized optical microscopy (POM) (Fig. 2e), yet lacking long-range order. Hence, we tried to anneal the poly(TAA) polymer at 120°C for 2 h to facilitate the chain mobility and reorganization without remarkably depolymerizing the polymer backbone (Fig. 2a and Supplementary Fig. 9,10). As a result, the polymer

melts reconstructed into highly crystalline spherulite domains with hundreds of micrometer diameters as observed by POM and scanning electron microscopy (SEM) (Fig. 2e and Supplementary Fig. 11,12). Differential scanning calorimetry (DSC) analysis confirmed the crystalline peaks at 61.2°C (Fig. 2c), and X-ray diffraction (XRD) analysis further disclosed the difference in order of the materials before and after the annealing process, referring to Am-poly(TAA) (amorphous) and Sc-poly(TAA) (semi-crystalline), respectively (Fig. 2f). Interestingly, the Sc-poly(TAA) showed similar yet different diffraction peaks with TAA monomers, reflecting their similar H-bond architectures, which was further verified by the highly consistent amide absorption bands between Sc-poly(TAA) and TAA crystals in ATR-IR spectra (Fig. 2d). Raman spectroscopy indicated the open-chain disulfide bonds in Sc-poly(TAA) (Extended data Fig. 1a), further evidencing the chemical nature of poly(disulfide)s.[27] To further distinguish the different H-bond crosslinking topologies between Sc-poly(TAA) and Am-poly(TAA), rheological curves were measured as a function of temperature (Fig. 2g). As a result, the Am-poly(TAA) material showed a typical thermoplastic feature with glass transition stage at 20°C, while the Sc-poly(TAA) material showing a softening stage starting from 60°C due to the melting of spherulite domains. Overall, these collective experimental data indicated the successful preparation of amorphous and semicrystalline poly(TAA) materials.

It is fundamentally interesting to study the H-bonding self-assembly of Sc-poly(TAA) when realizing the fact that almost all TA-based poly(disulfide)s form amorphous network.[28] To the best of our knowledge, the only existing example of semi-crystalline poly(disulfide)s based on TA derivatives was reported by Liu, et al.[29] by enabling tacticity in mainchain configuration via chemo-selective ROP at low temperature, which, unfortunately, was not used for material design. In this work, the high crystallinity of Sc-poly(TAA) materials came from sidechain self-assembly driven by forming robust reticular H-bonds of primary amides, instead of using catalyst to uniform the mainchain tacticity. To resolve the crystal

structure of Sc-poly(TAA), a set of microscopic techniques have been used to visualize the multi-length-scale order of the polymer chains. At micrometer level, the spherulite-like crystalline domains in Sc-poly(TAA) were imaged by POM, and further visualized by SEM as high-density stacking of cuboid polymeric crystals (Fig. 3a, 3b and Supplementary Fig. 11,12). High-resolution transmission electron microscope (HRTEM) showed the crystalline lattice and the electron diffraction pattern, indicating the high order of polymer chains at the nanoscale (Fig. 3c, 3d and Supplementary Fig. 13). Combining the ATR-IR and XRD results (Fig. 2d, 2f), we reasoned that the Sc-Poly(TAA) exhibited similar H-bonded architecture as seen with TAA monomers. Hence, we reconstructed the TAA single crystal structure into the crystal structure of Sc-Poly(TAA) by refining the disulfide bond linkages as well as energy optimization by molecular dynamics simulations (Fig. 3e, 3f; see details in Supplementary Materials). The optimized structure suggested a layered assembled architecture consisting of periodically stacking of poly(TAA) polymers in plane and intermolecularly crosslinked by forming H-bonds in a complicated reticular geometry (Fig. 3e). To further verify the crystal structures, synchrotron-radiation wide-angle X-ray scattering (WAXS) measurements were used to analyze the Am-Poly(TAA) and Sc-Poly(TAA) films, suggesting the remarkable enhancement of crystallinity after annealing process (Extended data Fig. 1b,1c, Fig. 3f, 3g and Supplementary Fig. 14). The peak at 17.3° was attributed to the order of distance (5.0 Å) between the neighboring oxygen atoms of amide-amide interactions at vertical z-direction, and the peaks at 15.3° were consistent with the periodic arrangement of the amide protons (5.9 Å) at the horizonal y-direction. By overlaying the experimental data with the simulated pattern from the reconstructed single-crystal structures, the good agreement confirmed their structural consistency (Fig. 3f).

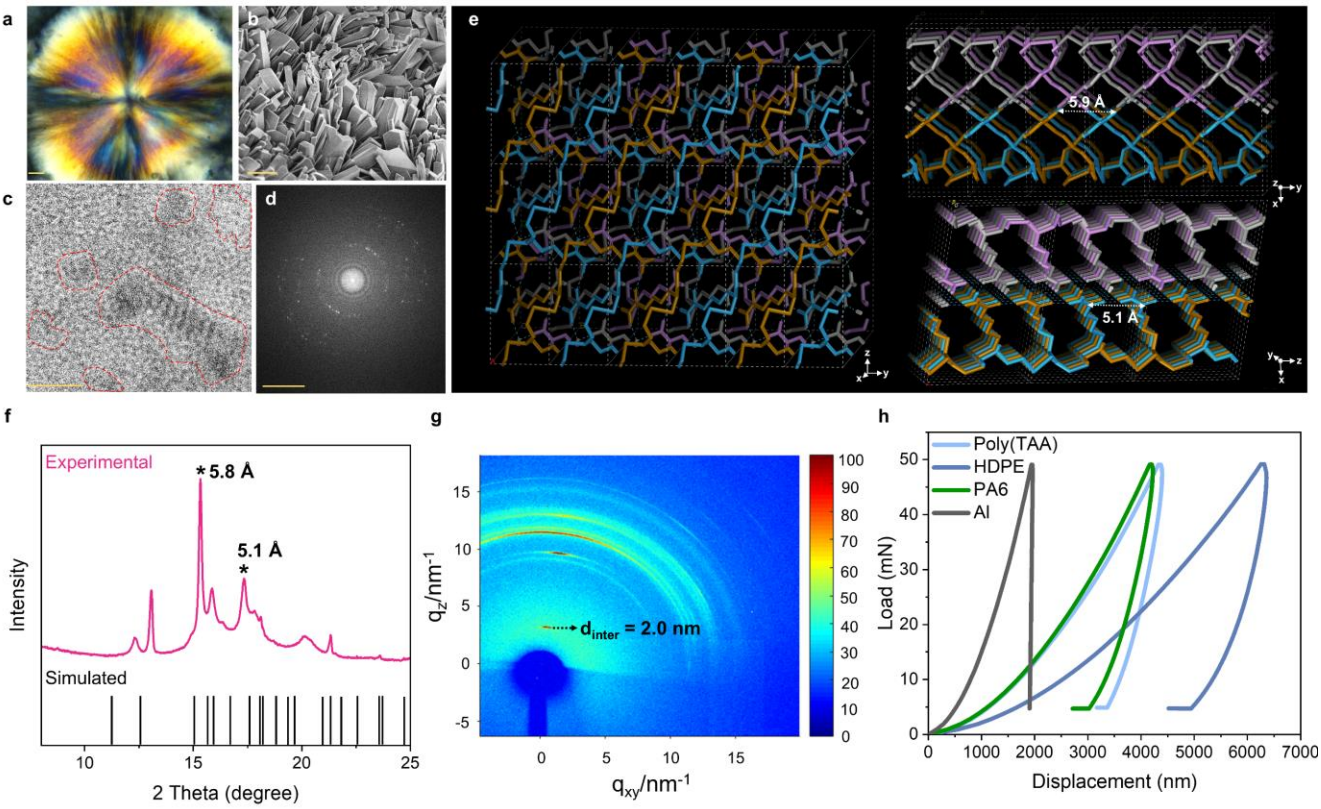

Fig. 3 | Structure Analysis of Semicrystalline Polymers and their Mechanical Performances. a, Microscopic images of the resulting Sc-Poly(TAA) polymers. Scale bar refers to 20 μm. **b**, SEM image of Sc-Poly(TAA) polymers. Scale bar refers to 5 μm. **c**, HRTEM image of Sc-Poly(TAA) polymers.The boundaries of the crystalline domain are marked with dashed red lines. Scale bar refers to 10 μm. **d**, Bright-field TEM image of Sc-poly(TAA). Scale bar refers to 2 nm^{-1}. **e**, Reconstructed solid-state crystal structures of Sc-poly(TAA) from different views (see detailed structural coordinates in Supplementary Informations). **f**, Overlay of simulated and experimental 1D WAXS data of Sc-Poly(TAA). **g,** Experimental 2D GIWAXS pattern of annealed poly(TAA) with large spherulites. **h**, Representative nano-indentation load-displacement curves of the semicrystalline poly(TAA). More than 24 indentation measurements have been performed in each sample to ensure the reliability of the results. Metallic aluminum: Al. Nylon-6: PA6. High-density polyethylene: HDPE.

Due to the high mechanical robustness, the mechanical properties of the Sc-Poly(TAA) polymers were evaluated by nano-indentation technique (Extended data Fig. 1d). From the load-displacement curves, the hardness (*H*) and Young's modulus (*E*) of Sc-Poly(TAA) polymers were measured as 0.11 ± 0.06 GPa and 2.90 ± 0.09 GPa, respectively (Fig. 3h and Extended data Fig. 1e). As a reference, three conventional

commercial engineering materials, e.g., metallic aluminum, Nylon-6 and high-density polyethylene (HDPE) were selected and measured under the same conditions. Remarkablely, the load-displacement curves showed that Sc-Poly(TAA) exhibited higher hardness and Young's modulus than HDPE, and very similar mechanical properties as Nylon-6, a typical semicrystalline engineering plastic also featuring ordered H-bonds (Extended data Fig. 1f and Supplementary Fig. 15). The Young's modulus of Sc-poly(TAA) is also comparable with other commercial polymers (Extended data Fig. 1g). To further understand the nanoscale modulus distribution, we performed nanomechanical imaging to investigated the surface/sub-surface mechanical properties of Sc-poly(TAA) by atomic force microscopy (Extended data Fig. 1h), yielding an averaged Young's modulus of 4.72 GPa. Therefore, it is concluded that Sc-poly(TAA) exhibited the highest robustness in all reported poly(disulfide)s,[25,26,28] mainly attributed to the synergistic strengthening effect of ordered H-bonds in the semicrystalline network.

Turning our attention to exploring the recyclability of Sc-poly(TAA) polymers to close the loop for circularity, we first checked the chemical recyclability of Sc-poly(TAA) polymer using conventional solvent-based methods, i.e., dilution-induced depolymerization. In a typical experiment, TFA was used to dissolve the Sc-poly(TAA) materials, resulting in the formation of yellow solution, the characteristic color of cyclic monomers. ^{1}H NMR spectra confirmed the quantitative depolymerization into TAA monomers (Supplementary Fig. 16). The separation and purification of TAA monomers required further solvent dilution and extraction to quench the acidity of TFA, followed by tedious solvent removal under vacuum and recrystallization. The overall recycling isolated yield of monomers was 85%, and the purity was confirmed by ^{1}H NMR (Supplementary Fig. 17). The loss of monomer during the separation is mainly attributed to the solvent extraction and recrystallization, which is unavoidable to obtain origin-quality crystalline monomers.

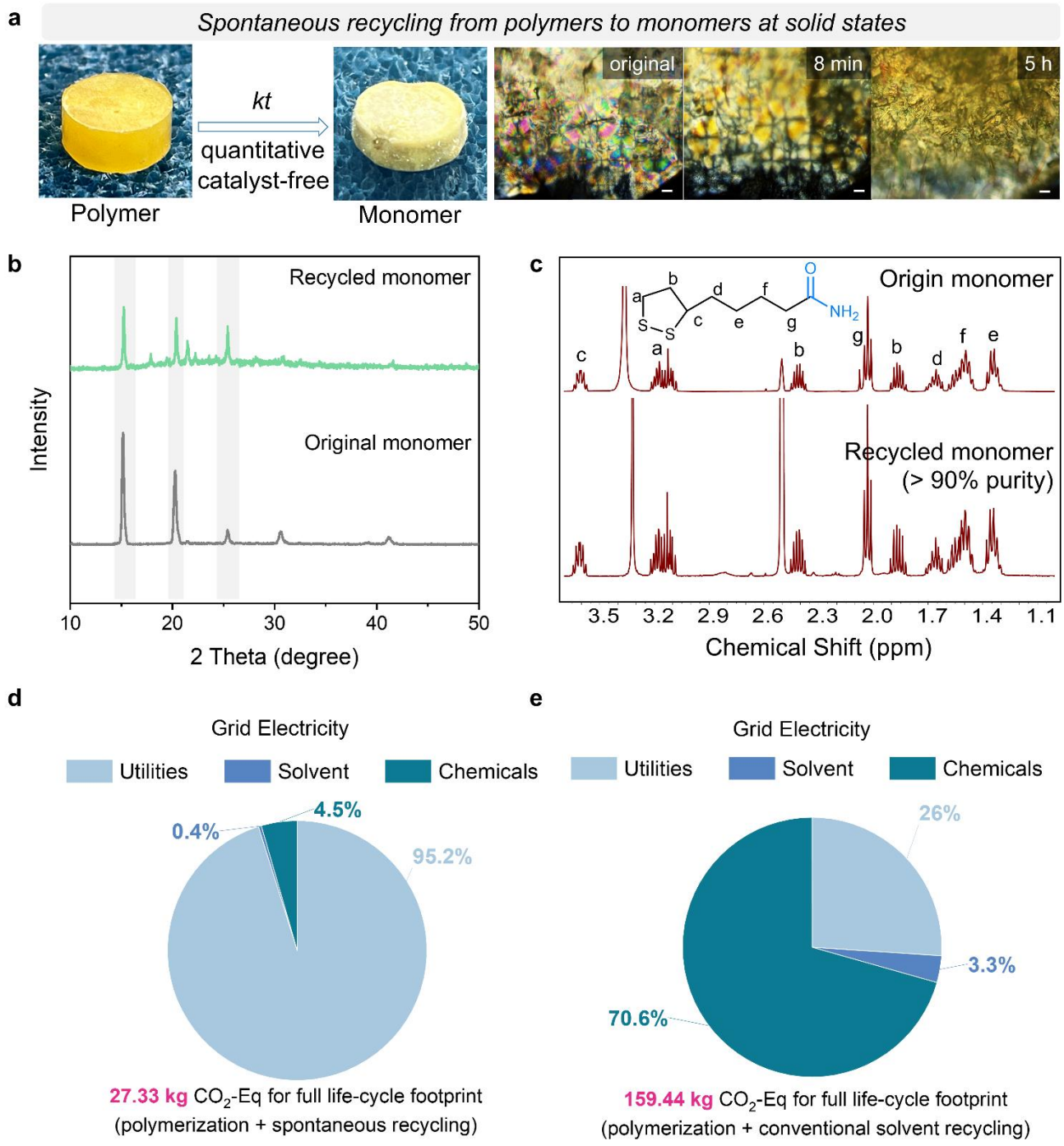

Fig. 4 | Polymer-to-Monomer Recycling in Solid States. a, Photographs and POM images of Sc-poly(TAA) materials before and after recycling by heating 120°C for given hours. Scale bar refers to 50 μm. **b**, XRD pattern comparison of the original TAA monomers and the recycled monomers. **c**, ^{1}H NMR spectra of the original TAA monomers and the recycled monomers in d_6-DMSO. **d** and **e**, Carbon footprint evaluated by life-cycle assessment of conventional solvent-based depolymerization and the spontaneous recycling in solid states (see details in Extended Fig. 3 and Supplementary Data).

Most interestingly, instead of using solvents or catalysts, simply annealing the Sm-poly(TAA) solids at 120°C for several hours drove the spontaneous conversion from translucent polymers into yellow powders with similar plate-like microcrystals of TAA monomers (Fig. 4a), which was further confirmed as TAA crystals by the consistent diffraction peaks in XRD (Fig. 4b and Supplementary Fig. 18–20). Comparing ^{1}H NMR analysis further confirmed the successful polymer-to-monomer conversion with quantitative yield and over 90% purity (Fig. 4c), which is a remarkable value for a solid-to-solid transition without the assistance of any solvent or catalyst. Trace amounts of oligomers coexisting within the recycled monomers should not affect the material regeneration in the next cycle because oligomers could also participate in the dynamic covalent equilibrium mediated by disulfide exchange. To further validate the generality of this concept, we carried out the recycling experiments on a series of TAA analogs with different H-bond geometries (Extended data Fig. 2 and Supplementary Fig. 21–27). For example, enantiopure RTAA showed a distinct packing manner due to the symmetry breaking and thus the 1,2-dithiolane rings were not spatially separated akin to TAA, which led to the relatively low efficiency of polymer-to-monomer conversion at solid states (Extended data Fig. 2a-2d and Supplementary Fig. 28,29). Another notable example was a TCA monomer, which bears a similar amide sidechain although without the alkyl linkage (Extended data Fig. 2e-2h and Supplementary Fig. 30). The single crystal structure of TCA monomers showed similar packing features as TAA. Upon polymerization by TFA solvation/desolvation cycle, poly(TCA) polymer was obtained as an amorphous network (Supplementary Fig. 31). Unlike Am-poly(TAA), annealing the amorphous poly(TCA) directly triggered the polymer-to-monomer recycling process by forming large-size single crystals from the amorphous network (Supplementary Fig. 32), further confirming the uniqueness of TAA molecular structure to feature kinetically trappable self-assembly of polymer chains as well as the spontaneous recycling capability at solid states (Fig. 1c).

To holistically evaluate the environmental footprint of full life cycle of this recycling system, we conducted life-cycle assessments (LCA)[30] of the two different routes both including production pathways and end-of-life management via conventional solvent-based recycling (P-CSR) versus the spontaneous recycling (P-SR) process (Extended data Fig. 3 and Supplementary Fig. S33–36). We first focused on the climate change indicator and analyzed the breakdown of the CO_2 footprint of the two processes. In the base scenario, utilities, e.g., electricity and electrified heating, contribute to 95% of the CO_2 footprint of the P-SR process (27.3 kg CO_2-eq) (Fig. 4d), whereas solvents and chemicals account for 70% of CO_2 footprint of the P-CSR process (159.44 kg CO_2-eq) (Fig. 4e), indicating the advantages of primary use of heat to recycle polymers in the case of P-SR. Further comparison by scoring the environmental footprint among seven indicators, the P-SR process bears 2.85 more points compared to the P-CSR process, with average 86.1% lower environmental footprint than P-CSR process on the basis of grid electricity (Extended Data Fig. 3). Considering the identical polymerization process for both routes, we conclude that it is the spontaneous recyclability responsible for the significant environmental benefits via solely requiring electricity for heating and avoiding the use of solvents and catalysts.

Towards future energy system, the P-SR route even has increasingly advantageous environmental benefits than the P-CSR process. Power grid decarbonization has long been viewed as a linchpin in the broader energy transition,[31] and highly-electrified processes, e.g., P-SR, can immediately benefit from rapid grid decarbonization to achieve further significant reduction in their environmental footprint. In a scenario that considers the use of wind electricity ("Wind Electricity" in Extended Data Fig. 3d, 3e), the P-SR process scores 5.31 more points than the P-CSR process on average among seven indicators, indicating that the former has on average 97.5% lower environmental footprint than the latter.

In summary, we introduce the concept of disequilibrating design into the scope of chemical recycling of dynamic polymers, enabling solid-to-solid depolymerization in bulk with enhanced energy and

environmental benefits. This strategy differs from conventional covalent design by featuring the key role of supramolecular control over the monomer-polymer equilibrium without engineering monomer structures, thus enabling an intrinsic dynamic way to recycle polymers acoiding the consuming of large quantities of energy and solvents. Notably, by elaborating the kinetic process of the H-bond self-assembly, it is also feasible to yield robust polymers i.e., strong rubber-like elastomers or semicrystalline polymers with mechanical modulus and hardness akin Nylon. We foresee that these discoveries could be a starting point for future easy recyclable yet robust polymers highlighting the significance of supramolecular chemistry approaches in the field of chemical recycling of synthetic polymers.[32–35]

Online content

Any methods, additional references, Nature Portfolio reporting summaries, source data, extended data, supplementary information, acknowledgments, peer review information; details of author contributions and competing interests; and statements of data and code availability are available at https://doi.org/XXXXXXXX.

References:

1. Zhu, J. B., Watson, E. M., Tang, J. & Chen, E. Y. X. A synthetic polymer system with repeatable chemical recyclability. *Science* **360**, 398–403 (2018).
2. Jehanno, C. *et al.* Critical advances and future opportunities in upcycling commodity polymers. *Nature* **603**, 803 (2022).
3. Zimmerman, J. B., Anastas, P. T., Erythropel, H. C. & Leitner, W. Designing for a green chemistry future. *Science* **367**, 397–400 (2020).
4. Lohmann, V., Jones, G. R., Truong, N. P. & Anastasaki, A. The thermodynamics and kinetics of depolymerization: what makes vinyl monomer regeneration feasible? *Chem. Sci.* **15**, 832–853 (2024).
5. Qin, B. & Zhang, X. On Depolymerization. *CCS Chemistry* **6**, 297–312 (2024).
6. Yang, S., Du, S., Zhu, J. & Ma, S. Closed-loop recyclable polymers: from monomer and polymer design to the polymerization–depolymerization cycle. *Chem. Soc. Rev.* **53**, 9609–9651 (2024).
7. Hong, M. & Chen, E. Y. X. Completely recyclable biopolymers with linear and cyclic topologies via ring-opening polymerization of γ-butyrolactone. *Nat. Chem.* 8, 42–49 (2015).
8. Odian, G. *Principles of Polymerization.* (John Wiley & Sons, Inc. 2004) doi:10.1002/047147875X.

9. Krause, S. Polymer Chemistry: An Introduction, 3rd Edition (Stevens, Malcolm P.). *J. Chem. Educ.* **77**, 35 (2000).

10. Whitfield, R., Jones, G. R., Truong, N. P., Manring, L. E. & Anastasaki, A. Solvent-free chemical recycling of polymethacrylates made by ATRP and RAFT polymerization: High-yielding depolymerization at low temperatures. *Angew. Chem. Inter. Ed.* **62**, e202309116 (2023).

11. Zhang, Q. *et al.* Dual closed-loop chemical recycling of synthetic polymers by intrinsically reconfigurable poly(disulfides). *Matter* **4**, 1352–1364 (2021).

12. Häußler, M., Eck, M., Rothauer, D. & Mecking, S. Closed-loop recycling of polyethylene-like materials. *Nature* **590**, 423–427 (2021).

13. Zhou, L. *et al.* Chemically circular, mechanically tough, and melt-processable polyhydroxyalkanoates. *Science* **380**, (2023).

14. Christensen, P. R., Scheuermann, A. M., Loeffler, K. E. & Helms, B. A. Closed-loop recycling of plastics enabled by dynamic covalent diketoenamine bonds. *Nat. Chem.* **11**, 442–448 (2019).

15. Lei, Z. *et al.* Recyclable and malleable thermosets enabled by activating dormant dynamic linkages. *Nat. Chem.* **14**, 1399–1404 (2022).

16. Abel, B. A., Snyder, R. L. & Coates, G. W. Chemically recyclable thermoplastics from reversible-deactivation polymerization of cyclic acetals. *Science* **373**, 783–789 (2021).

17. Wang, H. S., Truong, N. P., Pei, Z., Coote, M. L. & Anastasaki, A. Reversing RAFT polymerization: Near-quantitative monomer generation via a catalyst-free depolymerization approach. *J. Am. Chem. Soc.* **144**, 4678–4684 (2022).

18. Jones, G. R. *et al.* Reversed controlled polymerization (RCP): Depolymerization from well-defined polymers to monomers. *J. Am. Chem. Soc.* **145**, 9898–9915 (2023).

19. Zou, Z. *et al.* Rehealable, fully recyclable, and malleable electronic skin enabled by dynamic covalent thermoset nanocomposite. *Sci. Adv.* **4**, eaaq0508 (2018).

20. Wang, B. Sen *et al.* Acid-catalyzed disulfide-mediated reversible polymerization for recyclable dynamic covalent materials. *Angew. Chem. Inter. Ed.* **62**, e202215329 (2023).

21. Shi, C., Quinn, E. C., Diment, W. T. & Chen, E. Y. X. Recyclable and (Bio)degradable polyesters in a circular plastics economy. *Chem. Rev.* **124**, 4393–4478 (2024).

22. Shi, C. *et al.* Design principles for intrinsically circular polymers with tunable properties. *Chem* **7**, 2896–2912 (2021).

23. Rahimi, A. R. & Garciá, J. M. Chemical recycling of waste plastics for new materials production. *Nat. Rev. Chem.* **1**, 0046 (2017).

24. Sheldon, R. A. & Norton, M. Green chemistry and the plastic pollution challenge: towards a circular economy. *Green Chem.* **22**, 6310–6322 (2020).

25. Zhang, Q., Qu, D. H., Feringa, B. L. & Tian, H. Disulfide-mediated reversible polymerization toward intrinsically dynamic smart materials. *J. Am. Chem. Soc.* **144**, 2022–2033 (2022).

26. Deng, Y. *et al.* Acylhydrazine-based reticular hydrogen bonds enable robust, tough, and dynamic supramolecular materials. *Sci. Adv.* **8**, eabk3286 (2022).

27. Van Wart, H. E., Lewis, A., Scheraga, H. A. & Saeva, F. D. Disulfide bond dihedral angles from Raman spectroscopy. *Proc. Natl. Acad. Sci.* **70**, 2619–2623 (1973).

28. Albanese, K. R., Read de Alaniz, J., Hawker, C. J. & Bates, C. M. From health supplement to versatile monomer: Radical ring-opening polymerization and depolymerization of α-lipoic acid. *Polymer* **304**, 127167 (2024).

29. Du, T. *et al.* Controlled and regioselective ring-opening polymerization for poly(disulfide)s by anion-binding catalysis. *J. Am. Chem. Soc.* **145**, 27788–27799 (2023).

30. Guinée, J. B. *et al.* Life cycle assessment: Past, present, and future. *Environ. Sci. Technol.* **45**, 90–96 (2011).

31. Jenkins, J. D., Luke, M. & Thernstrom, S. Getting to Zero Carbon Emissions in the Electric Power Sector. *Joule* **2**, 2498–2510 (2018).

32. Aida, T. & Meijer, E. W. Supramolecular polymers – we've come full circle. *Isr. J. Chem.* **60**, 33–47 (2020).

33. Lehn, J. M. Dynamers: Dynamic molecular and supramolecular polymers. *Progress in Polymer Science (Oxford)* **30**, 814–831 (2005).

34. Roy, N., Schädler, V. & Lehn, J. M. Supramolecular polymers: Inherently dynamic materials. *Acc. Chem. Res.* **57**, 349–361 (2024).

35. L. Brunsveld, B. J. B. Folmer, E. W. Meijer, and R. P. S. & Laboratory. Supramolecular polymers. *Chem. Rev.* **101**, 4071–4097 (2001).

36. Kühne, T. D. *et al.* CP2K: An electronic structure and molecular dynamics software package-Quickstep: Efficient and accurate electronic structure calculations. *J. Chem. Phys.* **152**, (2020).

37. Becke, A. D. Density-functional exchange-energy approximation with correct asymptotic behavior. *Phys. Rev. A (Coll Park)* **38**, 3098 (1988).

38. Lee, C., Yang, W. & Parr, R. G. Development of the Colle-Salvetti correlation-energy formula into a functional of the electron density. *Phys. Rev. B* **37**, 785 (1988).

39. Goedecker, S. & Teter, M. Separable dual-space Gaussian pseudopotentials. *Phys. Rev. B* **54**, 1703 (1996).

40. Krack, M. Pseudopotentials for H to Kr optimized for gradient-corrected exchange-correlation functionals. *Theor. Chem. Acc.* **114**, 145–152 (2005).

41. Liu, D. C. & Nocedal, J. On the limited memory BFGS method for large scale optimization. *Math Program* **45**, 503–528 (1989).

42. Laio, A. & Parrinello, M. Escaping free-energy minima. *Proc. Natl. Acad. Sci. USA* **99**, 12562–12566 (2002).

43. Nosé, S. A unified formulation of the constant temperature molecular dynamics methods. *J. Chem. Phys.* **81**, 511–519 (1984).

44. Hoover, W. G. Canonical dynamics: Equilibrium phase-space distributions. *Phys. Rev. A (Coll Park)* **31**, 1695 (1985).

45. Ruiz, M. E. Documentation of changes implemented in the ecoinvent database v3.10 (2023.12.14).

46. Huijbregts, M. A. J. *et al*. ReCiPe2016: a harmonised life cycle impact assessment method at midpoint and endpoint level. *Inter. J. Life Cycle Assessment* **22**, 138–147 (2017).

Methods

Nanoindentation. Nanoindentation measurements were carried out in Anilent Nano Indenter G200 equipped with a diamond Berkovich tip at room temperature. The thermal drift was corrected to below 0.05 nm s^{-1}. The measurement includes a 10 s loading to 50 mN and then a 10 s unloading. The modulus and hardness were calculated by the NanoSuite software according to the collected data. More than 24 indentation measurements have been performed in each sample to ensure the reliability of the results.

Tensile analysis. Tensile tests were measured using an Instron 34TM-5 universal testing system equipped with a 100 N sensor. The data were recorded in real-time by a wire-connected computer system. Polymer films were cut into dog-bone shape with a width of 5 mm and an average thickness of 1 mm. Specimens were tested at a fixed tensile speed of 50 mm/min. Tensile measurement was carried out at ambient conditions for all samples, and each measurement was repeated with at least three independent specimens.

The polymerization process. In the polymerization process, 1 mL trifluoroacetic acid (TFA, $C_2HF_3O_2$) is added to dissolve the 1 g monomers. After 1 h, the gel-like mixture was dried under vacuum at room temperature. The yellow translucent polymer was soaked in methanol (CH_3OH) to remove the TFA residual and some unpolymerized monomers. The resulting white polymer was dried under vacuum at room temperature to get an amorphous polymer. The amorphous polymer was cured at 120°C for 2 h to obtain the semi-crystalline polymer.

Spontaneous recycling. The polymer was heated on a heating block at 120°C, during which the polymer

gradually depolymerized into monomers.

Solvent recycling. In the solvent recycling process, the polymers were first pulverized and then dissolved in TFA solvent. The monomer solution was diluted with ethyl acetate ($C_4H_8O_2$) to promote depolymerization, followed by the addition of aqueous sodium bicarbonate solution to neutralize the TFA. The aqueous phase was separated from the ethyl acetate phase, washed three times with ethyl acetate, and treated with zero liquid discharge to recover the water for further use. The combined ethyl acetate phase was evaporated at normal boiling point to yield the desired monomer, and the ethyl acetate vapor was condensed and recovered for further use.

Density functional theory (DFT). In this study, density functional theory (DFT) combined with the Atomic Simulation Environment (ASE) library was employed to refine the structural optimization and reaction kinetics of polymers. The CP2K-2024 software package served as the primary computational tool for these simulations[36]. The Becke, three-parameter, Lee-Yang-Parr (B3LYP) hybrid functional was utilized for accurate electronic structure calculations[37,38], along with an energy cutoff of 800 eV for the plane-wave basis set to ensure high computational accuracy. Goedecker-Teter-Hutter (GTH) pseudopotentials were used to describe the core electrons[39], while the Gaussian and Augmented Plane Waves (GAPW) method was employed for the valence electrons[40]. The L-BFGS (Limited-memory Broyden-Fletcher-Goldfarb-Shanno) optimization algorithm was implemented for structural refinement. This algorithm is well-suited for large systems due to its efficiency in handling the optimization of thousands of variables, which is essential for polymer systems[41]. The optimization process was followed by meta-dynamics (Meta-MD) simulations to explore the reaction pathways and kinetics. Meta-MD is a powerful enhanced sampling technique that allows the system to overcome energy barriers and explore a broader range of configurational space[42]. The Meta-MD simulations were conducted with a time step of 0.1 femtoseconds (fs) and the Nose-Hoover thermostat to maintain a constant temperature throughout the

simulations[43,44]. This setup ensures that the simulations capture the dynamic behavior of the polymer systems accurately over time. The reaction pathways were analyzed to determine the mechanisms and kinetic parameters governing the polymer reactions. This comprehensive approach combining advanced DFT calculations, efficient optimization algorithms, and enhanced sampling techniques provides detailed insights into the structural and kinetic properties of polymers, which are crucial for designing advanced polymeric materials.

Life Cycle Assessment

The *polymerization-recycle* processes evaluated in this work is illustrated in Extended Data Fig. 3a. In the *polymerization* process, trifluoroacetic acid (TFA, $C_2HF_3O_2$) is added to dissolve the monomers. The resulting monomer solution is then dried under vacuum, during which most of the TFA evaporates and a crude polymer is formed. The TFA vapor is condensed, recovered, and used in the next polymerization cycle. The crude polymer still contains residual TFA and some unpolymerized monomers, which are removed by soaking in methanol (CH_3OH). After the soaking, the clean polymer is separated from methanol by filtration and then sent for thermal treatment to obtain the desired polymers. The filtered methanol is neutralized by sodium bicarbonate ($NaHCO_3$), evaporated at normal boiling point, and recovered by condensation for further use. The solid residue from methanol recovery is washed with water dissolve sodium trifluoroacetate ($C_2F_3O_2Na$) and sodium bicarbonate so that water-insoluble monomers can be recovered by filtration and used in the next polymerization cycle. The filtered saline solution is treated with zero liquid discharge, where the water is recovered for further use and the salt is disposed of. In the *spontaneous recycling* process, end-of-life polymers are first pulverized. The resulting fine polymer powder is then used for thermal treatment to obtain the desired monomer. In the *conventional solvent recycle* processes, end-of-life polymers are first pulverized. The resulting fine polymer powder is then dissolved in TFA under continuously stirring. The monomer solution is diluted with ethyl acetate ($C_4H_8O_2$)

to promote depolymerization, followed by the addition of aqueous sodium bicarbonate solution to neutralize the TFA. The aqueous phase is separated from the ethyl acetate phase, washed three times with ethyl acetate, and treated with zero liquid discharge to recover the water for further use. The combined ethyl acetate phase is evaporated at normal boiling point to yield the desired monomer, and the ethyl acetate vapor is condensed and recovered for further use.

Mass and energy balance (MEB) calculations were performed for the above processes using experiment results (e.g., solvent and chemical consumptions), chemical engineering design principles (e.g., empirical electricity consumption for stirring), and a process simulation tool (Aspen Plus), to estimate the consumption of electricity, heat, water, methanol, ethyl acetate, sodium bicarbonate, and TFA. The consumption of monomers is not included in the MEB calculations because their losses can be minimized to negligible levels during the *polymerization-recycle* processes. We selected 1 kg polymer or 1 kg end-of-life polymer as the *functional unit* (FU), and converted the material and energy consumption values into *input feedstock intensity* (IFI), e.g., number of kWh electricity per FU. Detailed calculations, key assumptions, and tabulated consumption values are provided in the Supplementary Information (SI).

The goal of *life cycle assessment* (LCA) in this work is to a provide self-consistent comparison of the environmental footprints of the *polymerization-spontaneous recycling* (P-SR) process and the *polymerization-conventional solvent recycle* (P-CSR) process. The LCA was conducted in Microsoft Excel spreadsheet using Ecoinvent V3.10 database[45] (Cutoff System-Processes) and Recipe 2016 v1.03 midpoint (H) impact assessment method[46]:

$$EF_i = \sum IFI_j \times ef_j \qquad \text{Eqn.(1)}$$

Eqn (1) shows that, for any impact categories (i) defined by the Recipe midpoint method, the environmental footprint (EF) can be obtained by summing the product of input feedstock intensity (IFI)

and the emission factor (ef) for all material and energy consumption categories (j). Eqn (1) is indeed straightforward to use, but we believe there are three points worth explaining in more detail. First, the Recipe midpoint method has eighteen impact categories, and we focus on the seven categories most directly related to energy and the environment in the main text. They are acidification: terrestrial (kg SO_2-eq), climate change (kg CO_2-eq), energy resources: non-renewable (kg oil-eq), eutrophication: water (kg P-eq), land use (m^2∗a crop-eq), particulate matter formation (kg $PM_{2.5}$-eq), and water use (m^3). Next, any material and energy consumption category, there are usually multiple ef values in the Ecoinvent database. We chose ef values that correspond to production activities at the global level, so that our comparisons are not limited to a certain region. Finally, we considered two options for electricity, i.e., current grid electricity and wind electricity, and four options for heat, i.e., current grid electricity, wind electricity, coal, and natural gas, in our *EF* calculations. The current grid electricity was set as the calculation baseline because it is more readily available to industrial facilities than other energy sources.

The calculated *EF* values for the P-SR process and the P-CSR process show a difference around one order of magnitude, making a direct comparison on the plots visually challenging. Thus, we converted these *EF* values into environment beneficial scores using a logarithm-based rating system:

$$Score_i = \begin{cases} 7, \ for\ P-SR \\ 7 - \log_2 \frac{EF^{P-CSR}}{EF^{P-SR}}, for\ P-CSR \end{cases} \quad \text{Eqn.(2)}$$

In this rating system, a process with a lower *EF* in any impact category will receive a full score of 7 for that category. For each doubling of the EF in any category, 1 point will be deducted from the full 7 points. For example, in any category, if a process receives a score of 0, it has 2^7=128 times the *EF* value than another process that receives a score of 7. In this work, the *P-SR* process have lower *EF* in all impact categories than the *P-CSR* process and so receives a score of 7 in all categories. We provide tabulated original *EF* values in the SI.

Data availability

The authors declare that the data supporting the findings of this study are available within the paper and its Supplementary Information files or from the corresponding author upon request.

Acknowledgments:

This work was supported by the National Natural Science Foundation of China (grant nos. 22220102004, 22025503, 22475070, 22305083), Shanghai Municipal Science and Technology Major Project (grant no. 2018SHZDZX03), the Fundamental Research Funds for the Central Universities, the Program of Introducing Talents of Discipline to Universities (grant no. B16017), Science and Technology Commission of Shanghai Municipality (grant no. 21JC1401700), the Starry Night Science Fund of Zhejiang University Shanghai Institute for Advanced Study (grant no. SN-ZJU-SIAS-006), the Innovation Program of Shanghai Municipal Education Commission (2023ZKZD40), Shanghai Pujiang Program (grant no. 23PJ1402100, 23PJD020), China Postdoctoral Science Foundation (grant no. 2022TQ0105), Shanghai Sailing Program (grant no. 24YF2708400), the European Research Council (ERC; advanced grant no. 694345 to B.L.F.), the Dutch Ministry of Education, Culture and Science (Gravitation program No.024.601.035).

Author contributions

Q.Z., Y.D., D.H.Q. and B.L.F. conceived the project. Q.Z., D.H.Q. and B.L.F. supervised the research. Y.D. and L.L. carried out the synthesis, characterizations, and data acquisition. H.X.L. performed the life-cycle assessment. Q.Z., Y.D., H.X.L., L.L., B.L.F., D.H.Q., and H.T. analyzed the data and prepared the manuscript.

Competing interests

The authors declare the following competing interests: Y.X.D., L.L., Q.Z., and D.-H.Q. are inventors on a provisional patent application related to this work that has been filed by the East China University of

Science and Technology (serial no. 2024116246109, date: 14 November 2024). The authors that are not named in the patent declare no other competing interests.

Additional information

Supplementary information The online version contains supplementary materials available at https://doi.org/XXXXXXXX.

Extended Data

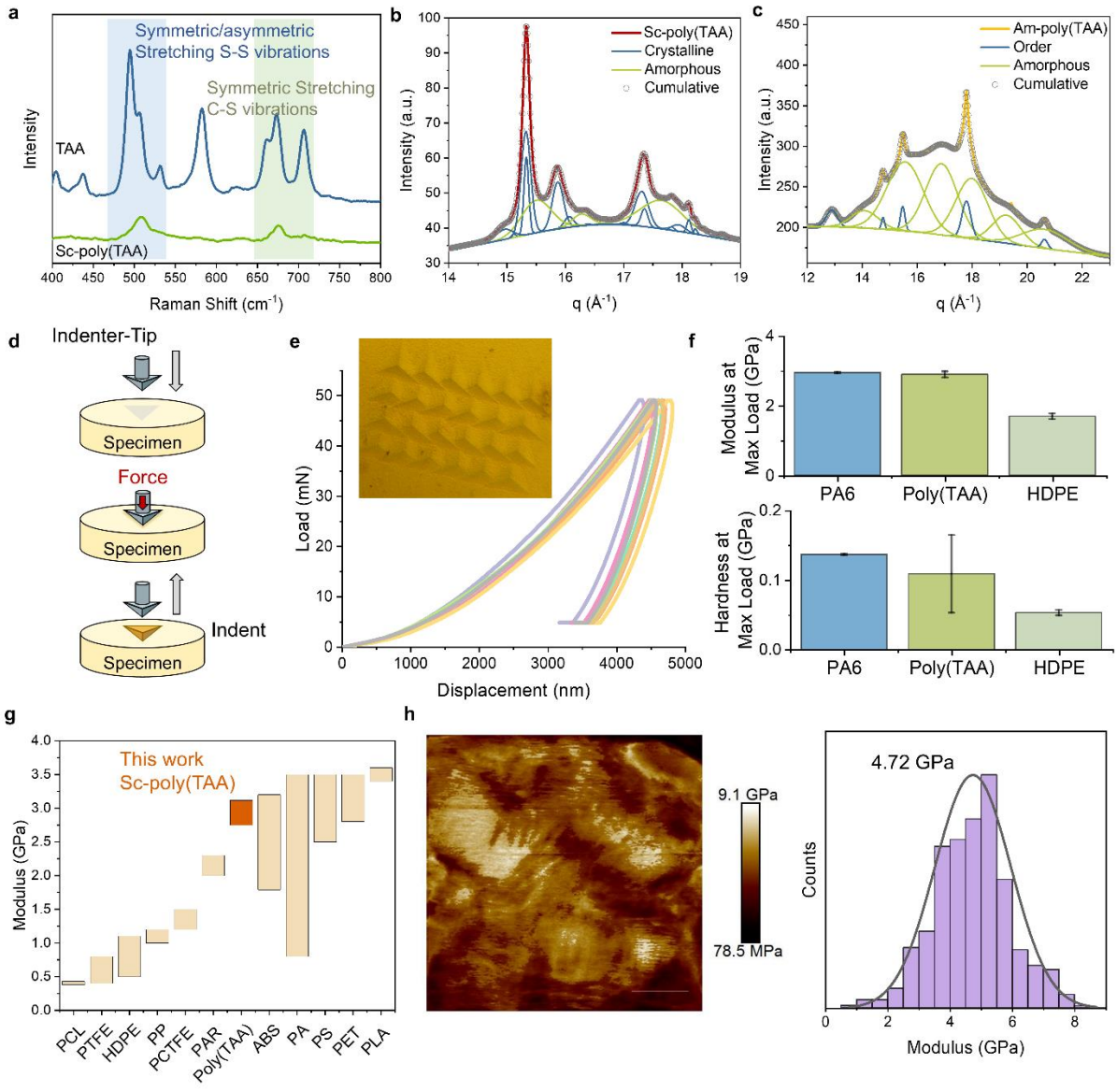

Extended Data Fig. 1 | Characterization and mechanical properties of Sc-poly(TAA). **a**, Partial Raman spectra of TAA monomer and crystalline Sc-poly(TAA). **b** and **c**, 1D-WAXS extracted radial profiles with the fitting of crystalline and amorphous phases of Sc-poly(TAA) and Am-poly(TAA). **d**, Schematic representation of the nano-indenter measurement. **e**, Representative nano-indentation load-displacement curves of Sc-poly(TAA). 30 indentation measurements have been performed to ensure the reliability of the results. **f**, Modulus and hardness of Nylon-6, Sc-poly(TAA), and HDPE. Nylon-6: PA6. High-density polyethylene: HDPE. **g**, Comparision of Sc-poly(TAA) and other commercial polymers. **h**, PeakForce quantitative nanomechanics measurement of Sc-poly(TAA).

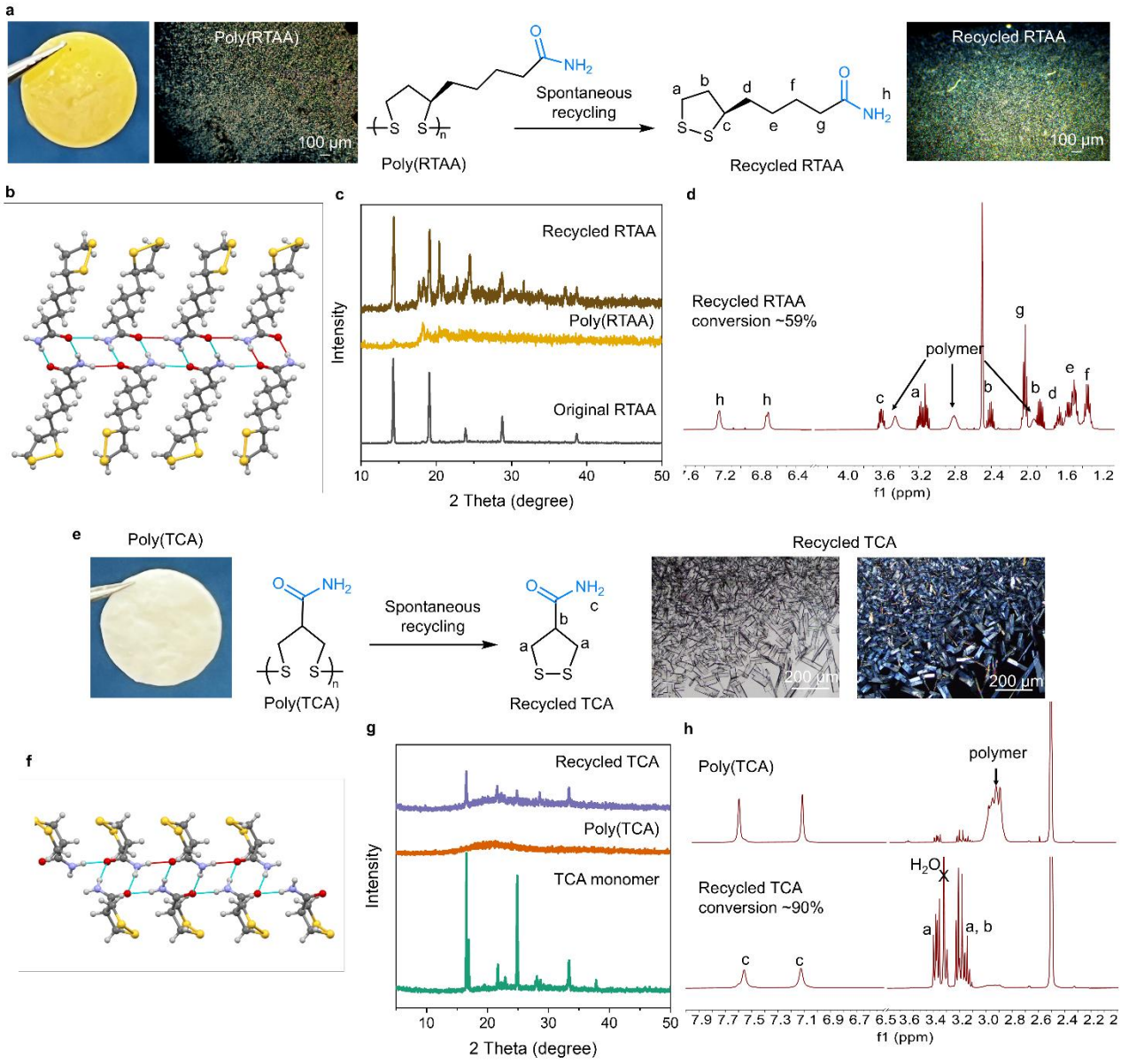

Extended Data Fig. 2 | Solid-state recycling of poly(TCA) and poly(RTAA). **a**, Photograph of poly(RTAA) after annealing. POM images of poly(RTAA) and recycled RTAA. **b**, X-ray single-crystal of RTAA. View along *a* axle to show the H-bond network of the amide unit. **c**, XRD pattern of RTAA monomer, poly(RTAA) catalyzed by TFA, and recycled RTAA. **d**, ^{1}H NMR spectra of recycled RTAA showing a monomer conversation around 59%. **e**, Photograph of poly(TCA) catalyzed by TFA. Bright field and POM image of recycled TCA. **f**, X-ray single-crystal of TCA. View along *b* axle to show the H-bond network of the amide unit. **g**, XRD pattern of TCA monomer, poly(TCA) catalyzed by TFA, and recycled TCA. **d**, ^{1}H NMR spectra of poly(TCA) and recycled RTAA showing a monomer conversation around 90%.

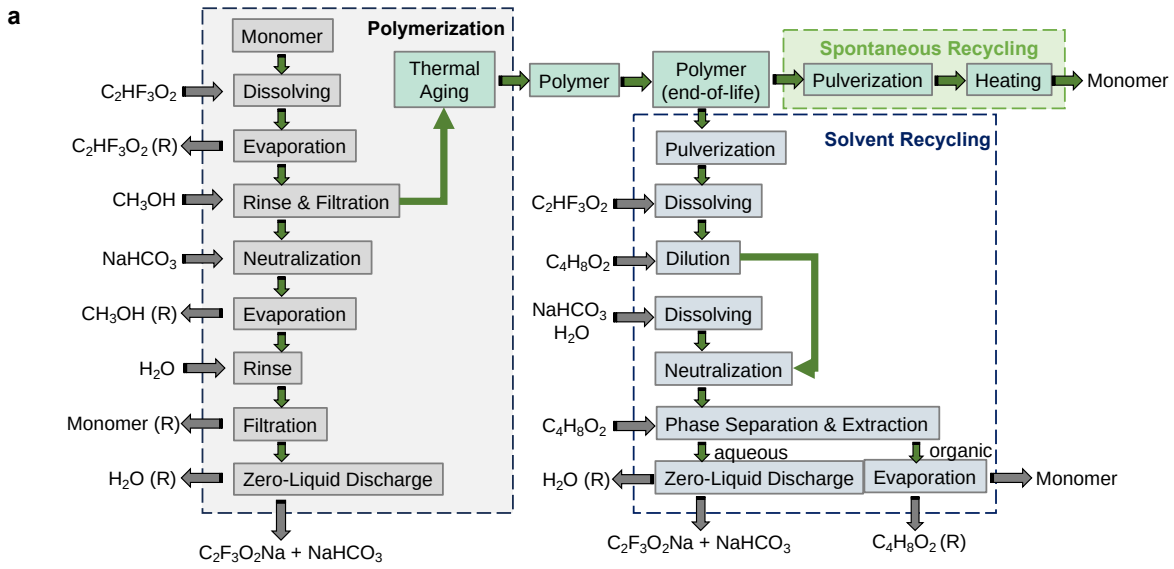

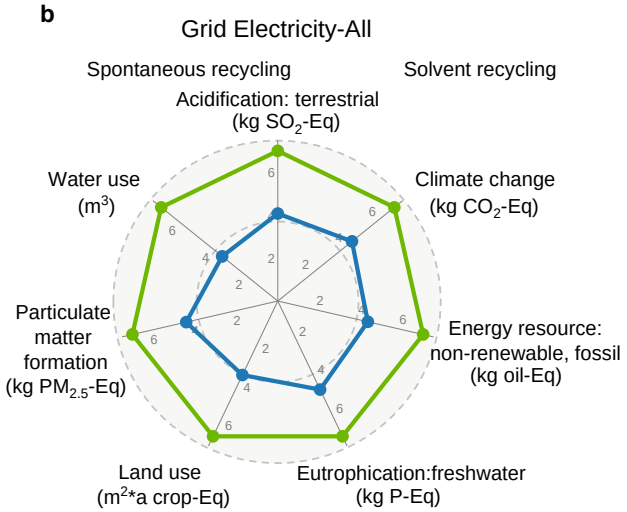

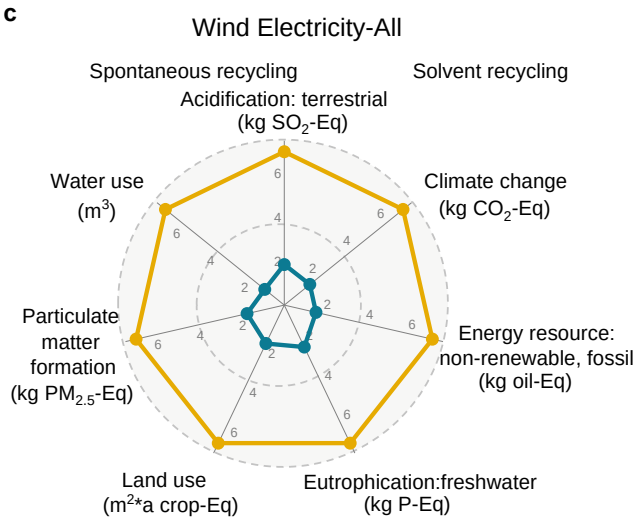

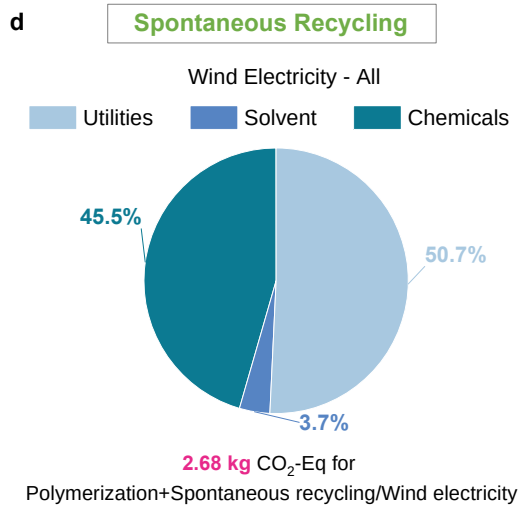

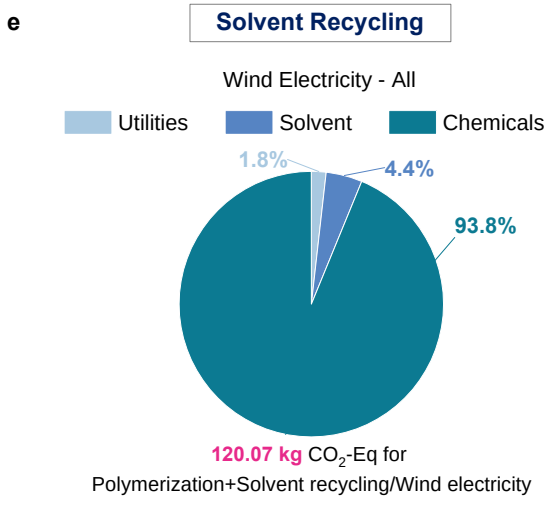

515

Extended Data Fig. 3 | Life cycle assessment of spontaneous recycling and solvent recycling of poly(TAA). a, The flow chart of polymerization, spontaneous recycling, and solvent recycling process. **b** and **c**, Environmental evaluation between spontaneous recycling in bulk and conventional dilution-induced depolymerization based on different electricity source. P: phosphorus. **d** and **e**, Environmental footprints of polymerization+solvent recycling process and polymerization+solid-state recycling process considering using wind electricity.